SUPPLEMENTARY MATERIAL

Multi-proxy crossdating extends the longest high-elevation tree-ring chronology from the Mediterranean

P. Römer, F. Reinig, O. Konter, R. Friedrich, O. Urban, J. Čáslavský,

N. Pernicová, M. Trnka, U. Büntgen and J. Esper

Table A1. ^{14}C and $\delta^{13}C$ dating results of specimen Pine44b.

Ring	$F^{14}C \pm \sigma$	C^{14} age ± σ	Unmodeled		Modeled		$\delta^{13}C$	$\delta^{13}C$ date
			from	to	from	to		
699	0.8499 ± 0.0020	1307 ± 19	656	777	**688**	**711**	-20.71	**699**
700	0.8497 ± 0.0020	1308 ± 19	656	777	**689**	**712**	-21.02	**700**
701	0.8498 ± 0.0021	1308 ± 19	656	777	**690**	**713**	-21.45	**701**
772	0.8472 ± 0.0021	1332 ± 18	646	778	**761**	**784**	-20.79	**772**
773	0.8487 ± 0.0021	1318 ± 19	651	778	**762**	**785**	-20.42	**773**
774	0.8533 ± 0.0021	1275 ± 19	661	829	**763**	**786**	-20.95	**774**
775	0.8592 ± 0.0021	1219 ± 19	685	890	**764**	**787**	-20.74	**775**
776	0.8656 ± 0.0022	1159 ± 19	771	986	**765**	**788**	-20.76	**776**
777	0.8633 ± 0.0021	1181 ± 19	770	973	**766**	**789**	-20.56	**777**
820	0.8554 ± 0.0021	1255 ± 19	669	879	**809**	**832**	-20.17	**820**
999	0.8793 ± 0.0021	1034 ± 19	899	1040	**988**	**1011**	-	-
1000	0.8771 ± 0.0021	1054 ± 19	895	1034	**989**	**1012**	-	-
1001	0.8779 ± 0.0021	1046 ± 19	896	1035	**990**	**1013**	-	-

Ring: TRW-based dates CE, **$F^{14}C$:** Normalized ^{14}C activity ratios (± 1σ), **^{14}C age:** Uncalibrated ^{14}C ages BP (± 1σ), **Unmodeled:** Individually calibrated ^{14}C age ranges CE (3σ; 99.7% probability), **Modeled:** Wiggle-matched ^{14}C age ranges CE (3σ; 99.7% probability), **$\delta^{13}C$:** Stable carbon isotope ratios [‰], **$\delta^{13}C$ date:** $\delta^{13}C$-derived dates CE.

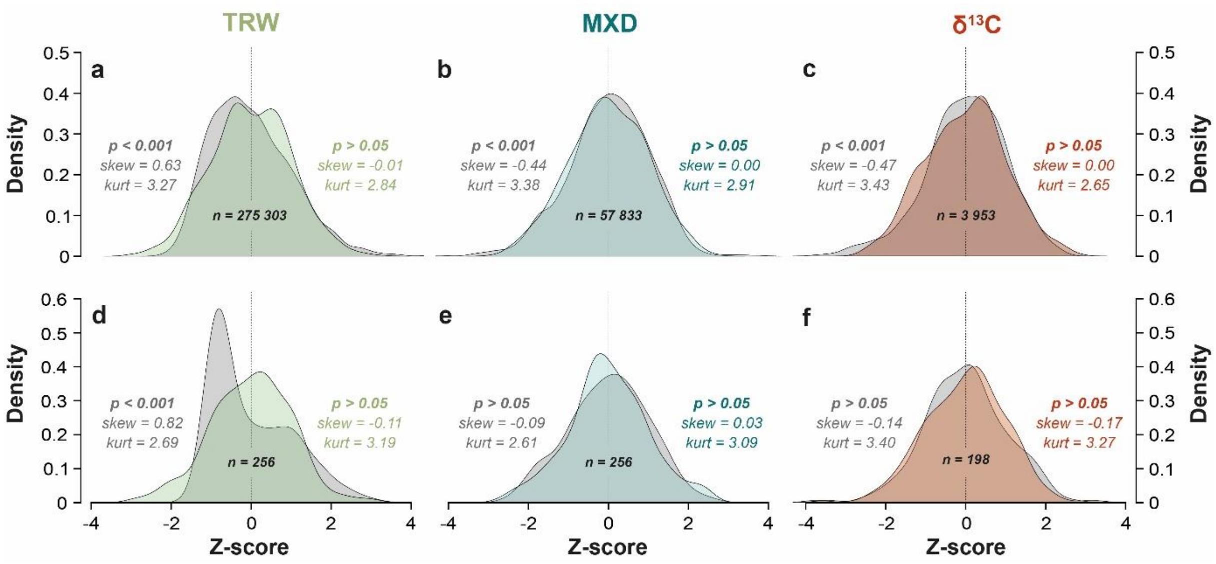

Fig. A1. Effects of high-pass filtering. Distribution of z-scored proxy data for **(a-c)** the entire dataset and for **(d-f)** Pine16a. Probability density of the raw (gray) and detrended (color) data with Shapiro-Wilk test results (p-values), skewness (skew), kurtosis (kurt), and sample size (n; total number of rings). Note that high-pass filtering pushes the data closer to normal distribution and largely reduces skewness and kurtosis, especially in the large datasets (a-c).

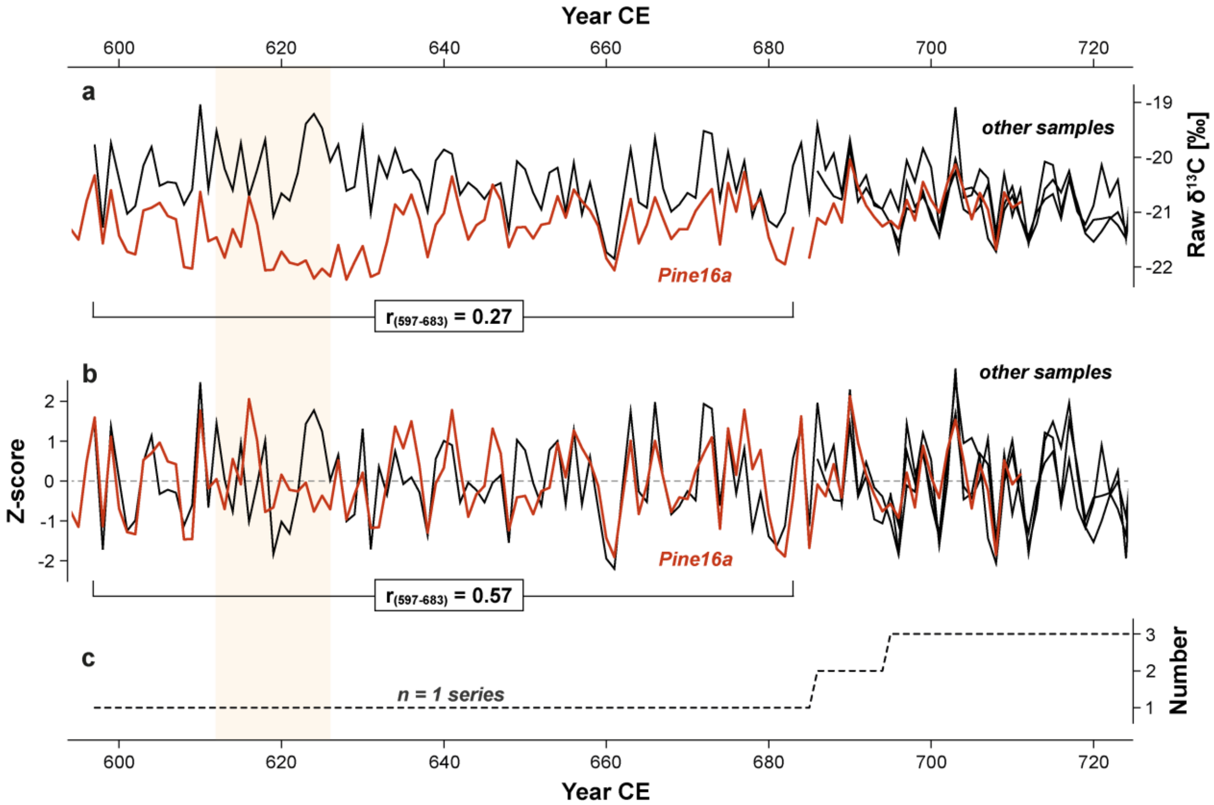

Fig. A2. Pine16a at Opt2 (468–723 CE). **(a)** Raw and **(b)** high-pass filtered $\delta^{13}C$ series with corresponding Pearson correlations between Pine16a and the master chronology when n = 1 series (597–683 CE). Note the strong covariance between the two time series. The yellow area in the background highlights a short period (613–625 CE) of high-frequency mismatch. **(c)** Sample replication of the $\delta^{13}C$ chronology.

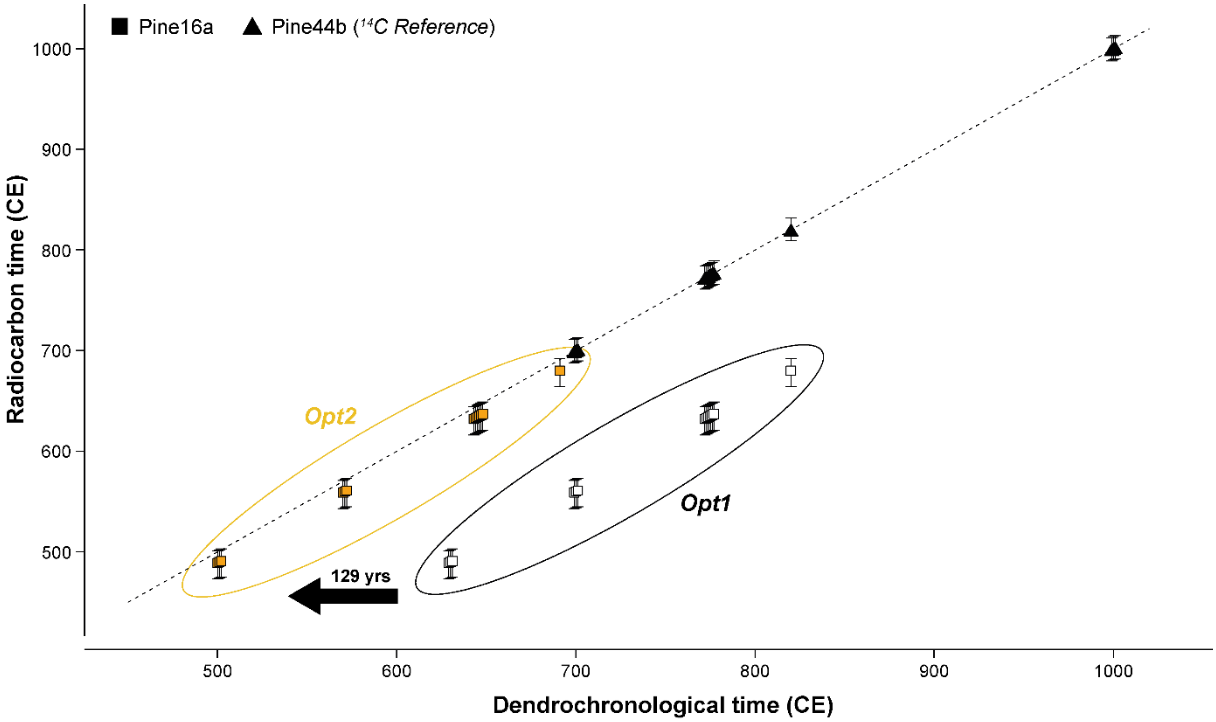

Fig. A3. Independent age validation with ^{14}C. Symbols represent the mean calendric ages CE of the ^{14}C wiggle-match and whiskers the age ranges at 99.7% probability. The dashed line denotes similar years between calibrated ^{14}C ages and dendrochronological dates. Note that Pine44b and Opt2 whiskers consistently overlap with the dashed line and are therefore considered correct.

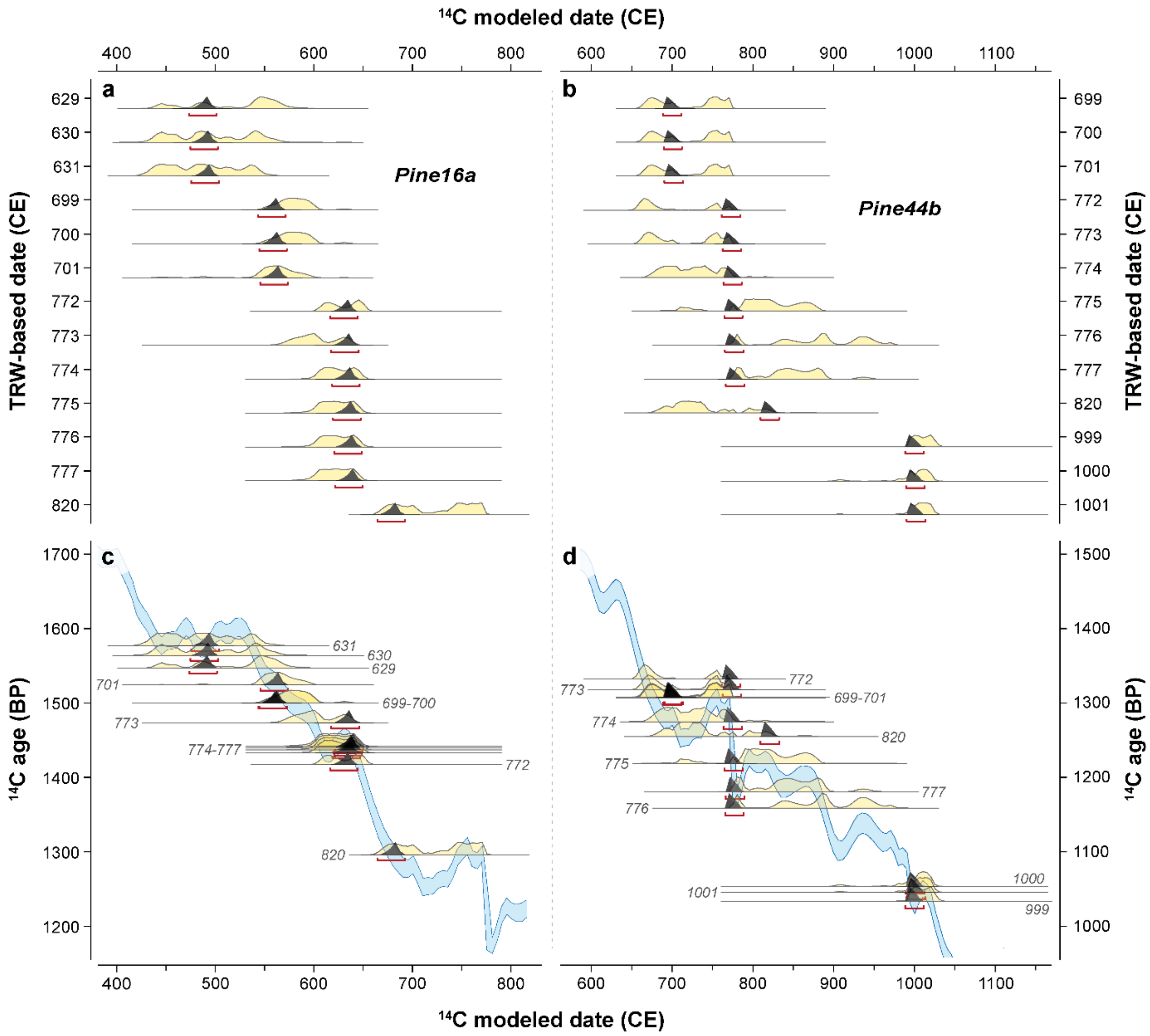

Fig. A4. OxCal results of **(a)** Pine16a and **(b)** Pine44b. The individual tree rings are coded by their TRW-based dates. Smoothed histograms represent the probability distributions of the individual (yellow) and wiggle-match (gray) age ranges (CE) at 99.7% probability. The wiggle-match results are highlighted by red brackets. Uncalibrated ^{14}C ages (BP) of (**c**) Pine16a and **(d)** Pine44b plotted against IntCal20.